ELSEVIER

Global and Planetary Change 19 (1998) 225–240

GLOBAL AND PLANETARY CHANGE

Eastern Asian hydrometeorology simulation using the Regional Climate System Model

Jinwon Kim [a,*], Norman L. Miller [a,1], Jai-Ho Oh [b,2], Jun-Seok Chung [b,3], Deukkyun Rha [b,4]

[a] *University of California, Lawrence Livermore National Laboratory, P.O. Box 808, Livermore, CA 94551, USA*
[b] *Meteorological Research Institute / Korean Meteorological Administration, Seoul, South Korea*

Received 30 July 1997; accepted 9 February 1998

Abstract

We present the hydrometeorology of eastern Asia during April 1995 simulated by the Regional Climate System Model. The amount and location of simulated monthly precipitation agrees well with observations. Soil water content variation was closely correlated with precipitation. Land-surface evaporation and the surface energy budget were strongly controlled by soil moisture content. A sensitivity test with reduced initial soil moisture content suggested that near-surface soil moisture spins up quickly after heavy precipitation events. However, variations in the initial soil moisture field may alter details of the simulated precipitation which can introduce further complexity in climate simulations. © 1998 Elsevier Science B.V. All rights reserved.

Keywords: regional climate system model; coupled atmosphere—land surface model; East Asian hydroclimate; sustainability

1. Introduction

Regional climate and its variation exert significant impacts on human lives and natural ecosystems. It affects the available water resources, flood and drought potentials, and agricultural productivity. Hence, assessment of climate variability and its regional impacts is important for planning sustainable development. The significance of hydroclimate impacts on society and environments has made regional hydroclimate research one of the main focus areas of global climate research programs (e.g., GEWEX).

Regional climate is a consequence of complex interactions among physical and dynamical processes at various temporal and spatial scales, ranging from climatological modulation of planetary-scale circulations to the local elements such as terrain slope, vegetation, and the presence of lakes. The main goals of regional climate modelling include understanding the interactions among these processes, determining the sensitivity of regional processes to large-scale forcing, and providing an improved re-

* Corresponding author. Present address: University of California, Lawrence Berkeley National Laboratory, 1 Cyclotron Road, Berkeley, CA 94720, USA. Fax: +1 510 486 7070. E-mail: Jinwon_Kim@LBL.gov

[1] Present address: University of California, Lawrence Berkeley National Laboratory, 1 Cyclotron Road, Berkeley, CA 94720, USA. Fax: +1 510 486 7070. E-mail: nlmiller@LBL.gov.

[2] Fax: 82-2-763-8209; jho@iris.metri.re.kr.

[3] Fax: 82-2-763-8209; cjs@iris.metri.re.kr.

[4] Fax: 82-2-763-8209; dkrha@iris.metri.re.kr.

0921-8181/98/$ - see front matter © 1998 Elsevier Science B.V. All rights reserved.
PII: S0921-8181(98)00049-6

gional climate prediction capability. Physically-based limited-area models nested within the large-scale fields are important tools for such purposes. In recent years, a number of groups have worked toward the formulation of regional climate models based on nested mesoscale models (e.g., Dickinson et al., 1989; Pielke et al., 1992; Giorgi et al., 1994; Giorgi, 1995; Kim et al., 1997). Studies by Giorgi and Bates (1989) and Giorgi et al. (1993) showed that a regional climate model can produce more realistic regional features compared to GCM simulations.

Interaction between the atmosphere and land surface is an important determinant of regional climate. Evaporation from land surfaces is one of the major sources of water vapor for extratropical convection (Mintz, 1984). Soil moisture and vegetation strongly affect local energy and water exchange between the atmosphere and land surface (Cuenca et al., 1996; Kim and Ek, 1995). Land-surface heterogeneity can generate mesoscale circulations that may significantly affect precipitation and local surface energy budgets (e.g., Fast and McCorcle, 1991; Avissar and Pielke, 1989; Miller, 1995).

Improvements of the land-surface component of regional and global climate models have recently become an area of intense research (Dickinson et al., 1991, Henderson-Sellers and Pitman, 1992). Compared to the early bucket-type models (Manabe, 1969), the new generation of land-surface models include extensive physical processes for moisture and heat transfer within near-surface soil layers, snow budget, vegetation effects, evolution of vegetation characteristics, and carbon cycle (e.g., Mahrt and Pan, 1984, Dickinson et al., 1986, Sellers et al., 1986; Pitman, 1988; Pan, 1990; Jacquemin and Noilhan, 1990; Kim and Ek, 1995). The significance of atmosphere–land surface interactions made evaluation and improvements of coupled atmosphere–land surface models a major topic for the Project for Intercomparison of Land-surface Parameterization Schemes (PILPS) Phase 4 experiments (Timbal et al., 1996).

The Regional Climate System Model (RCSM: Miller and Kim, 1996; Kim et al., 1997; Miller et al., 1997) was developed for physically-based modelling of regional climate, its variability, and impact assessments. One of the main functions of the RCSM is to downscale large-scale climate and weather information to watershed scales for hydrologic modelling and assessment. The RCSM is composed of a pre-processor, process models, and a post-processor (Fig. 1). The pre-processor produces input data for process

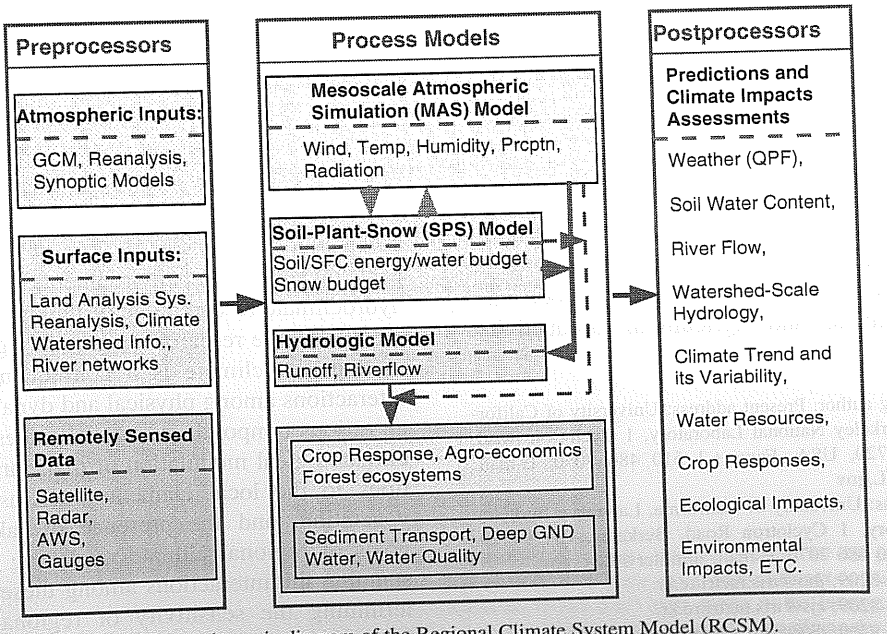

Fig. 1. A schematic diagram of the Regional Climate System Model (RCSM).

models using large-scale analyses and local observations, surface characteristics for hydrologic models, and geographical information needed for nesting. The process models include the Mesoscale Atmospheric Simulation (MAS) model (Kim and Soong, 1996, Soong and Kim, 1996), the Soil—Plant—Snow (SPS) model (Kim and Ek, 1995), a lumped (Sacramento model: Bae and Georgakakos, 1994) and distributed (TOPMODEL: Beven et al., 1994) hydrologic models. Crop production and impact assessment models are currently being included in collaboration with NCAR and NASA scientists. The process model results are archived, analyzed, and visualized by the post-processor.

The main focus of this study is the simulation of precipitation and soil moisture fields during a spring planting season and an investigation of soil moisture spin up during the simulation. The next section provides a description of the coupled MAS–SPS model, followed by results from an eastern Asian hydroclimate study and a sensitivity experiment due to initial soil moisture content.

2. The coupled MAS–SPS model

The coupled MAS–SPS model is the core modelling component of the RCSM. Fig. 2 schematically illustrates heat and water exchange between the atmosphere and a land surface in the MAS–SPS model. The land surface is a hypothetical composite including bare soil, free water, and a single layer canopy. Contribution from each surface element is accounted by the fraction of the surface area covered by individual elements. Downward short- and longwave radiation and precipitation are computed by the MAS model. Upward longwave radiation and turbulent heat transfer between land surfaces and the atmosphere are computed by iteratively solving a nonlinear form of the surface energy balance equation (Kim and Ek, 1995).

2.1. The mesoscale atmospheric simulation (MAS) model

The MAS model is a primitive-equation limited area model with the σ-coordinate in the vertical. We utilized an 18-layer version of the MAS model in this study. The dependent variables are staggered on the Arakawa-c grid in the horizontal and on the Lorenz grid (Lorenz, 1960) in the vertical, respectively. The advection equation is solved using the third-order accurate finite–difference scheme by Takacs (1985), which causes a negligible phase error and small numerical dispersion. Non-advective vertical differencing of the dependent variables follows Arakawa and Suarez (1983). The vertical eddy transfer at the lower boundary is computed using the bulk aerodynamic scheme by Deardorff (1978). The calculated surface drag coefficients are also used in the SPS model to solve the surface energy balance equation and to compute the resistance of surface vegetation. Vertical eddy transport above the surface is computed using the K-theory, where the eddy diffusivities are computed using the formulation of Louis et al. (1981) with parameters estimated by Kim and Mahrt (1992). The time-dependent forcing from the large-scale data is prescribed along the lateral boundaries using the relaxation scheme by Davies (1976).

The grid-scale condensation and precipitation are computed using the four-class version of the bulk cloud microphysics scheme of Cho et al. (1989). This modified scheme neglects the microphysical processes associated with graupel, as sensitivity tests suggest that graupel does not have a significant contribution toward simulating precipitation and radiation at resolutions coarser than 10 km. Convective precipitation is calculated by the cumulus parameterization by Anthes (1977). To ensure the conservation of total water, the grid-scale condensation and convective precipitation calculations are coupled such that the moisture field adjusted by convection is used to compute microphysical interactions. For this coupling, the original scheme of Anthes (1977) was modified in such a way that the amount of convective condensation is added to the existing hydrometeors at each model level following the heating rate. The updated hydrometeor and water-vapor fields are used to compute microphysical interactions. This method ensures conservation of total water and energy due to phase changes. It also significantly reduced the occurrence of numerical point storm events (Giorgi, 1991). One important advantage of an explicit microphysics scheme is that cloud optical properties are directly computed for radiation calculations. This can eliminate uncertainties in the radia-

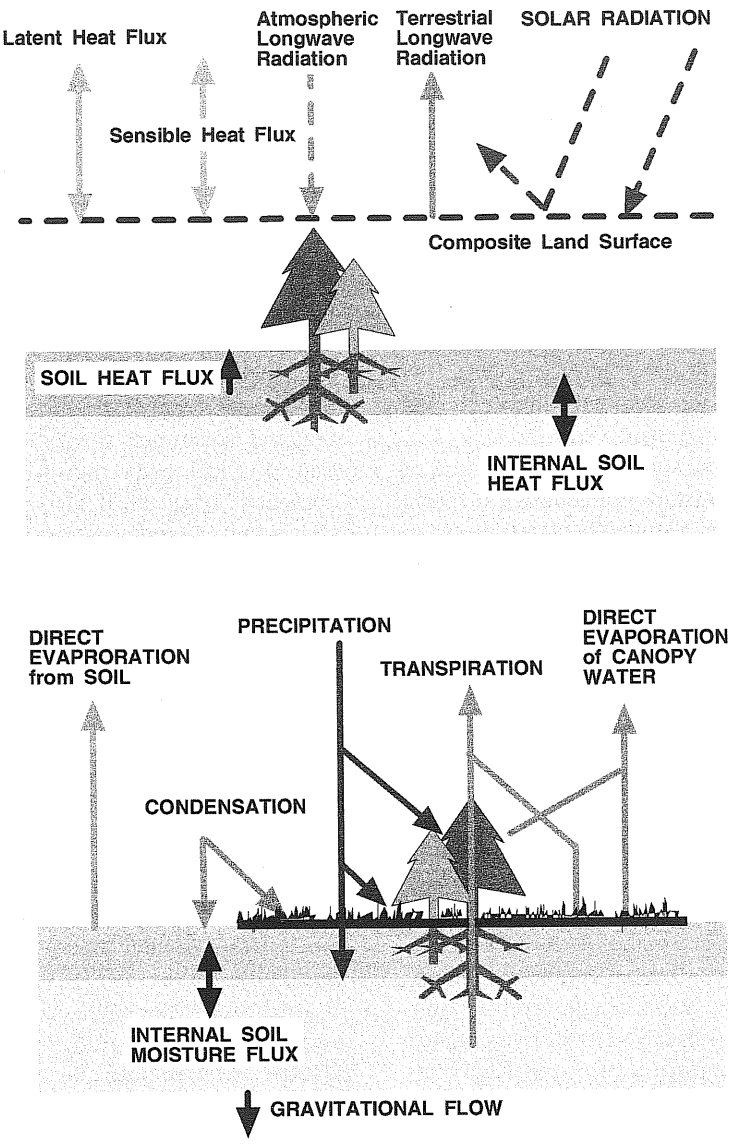

Fig. 2. A schematic representation of the energy and water exchange between the land surface and atmosphere included in the coupled MAS–SPS model (courtesy of M. Ek).

tive forcing that is the major energy input to the land-surface processes.

The solar and terrestrial radiation are computed following Harahvardahn et al. (1987) after effects of ice and water clouds for solar (Stephens, 1978) and terrestrial (Starr and Cox, 1985) radiative transfer are included. The 7-band solar radiation scheme uses the Delta–Eddington approximation for a large optical thickness and a two-stream approximation for a small optical thickness. The terrestrial radiative transfer scheme is based on the bulk emissivity of atmospheric layers.

2.2. The soil–plant–snow (SPS) model

We used a two-layer version of the SPS model (Kim and Ek, 1995) that originated from the soil-

plant–snow part of the Oregon State University's Coupled Atmosphere Plant Snow (CAPS) model (Mahrt and Pan, 1984, Pan and Mahrt, 1987). The thickness of the upper and lower soil layers was set to 5 cm and 195 cm, respectively, in this simulation. The SPS model predicts volumetric soil moisture content, soil temperature, canopy water content, and water-equivalent snow depth. The skin temperature and water vapor mixing ratio, which are used for computing heat and water vapor exchange between the atmosphere and land surfaces, are computed from the surface energy balance equation.

The governing equations for volumetric moisture content (Q) and temperature (T) for each soil layer and canopy water content (W_c) are:

$$\frac{\partial Q}{\partial t} = \frac{\partial}{\partial z}\left[K_Q \frac{\partial Q}{\partial z}\right] + \frac{\partial D}{\partial z} + F_Q \quad (1)$$

$$C\frac{\partial T}{\partial t} = \frac{\partial}{\partial z}\left[K_T \frac{\partial T}{\partial z}\right] + F_T \quad (2)$$

$$\frac{\partial W_c}{\partial t} = P - D_r - E_c \quad (3)$$

where D is the hydraulic conductivity (ms^{-1}), K_Q is the soil moisture diffusivity ($m^2\ s^{-1}$), K_T is the soil heat conductivity ($Wm^{-1}\ K^{-1}$), C is the soil heat capacity ($Jm^{-3}\ K^{-1}$), P is precipitation, D_r is water dripping from canopy, and E_c is evaporation of canopy water. F_Q and F_T are source and sink terms for soil moisture and soil temperature, respectively. These include infiltration, evapotranspiration, subsurface runoff, drainage, exfiltration, and transport of sub-surface water and soil heat across the lateral boundaries of a soil column. Eqs. (1) and (2) apply to the two soil layers and Eq. (3) applies to the single canopy layer.

Surface fluxes of heat and moisture are determined by solving a nonlinear form of the surface energy balance equation:

$$R^{\downarrow} - \varepsilon\sigma T_s^4 - H - L - G = 0 \quad (4)$$

where $R^{\downarrow}$ is the sum of downward solar and terrestrial radiation at land surfaces (Wm^{-2}), T_s is the skin temperature (K), H is the sensible heat flux (Wm^{-2}), L is the latent heat flux (Wm^{-2}), ϵ is the emissivity of the land surface, σ is the Stefan–Boltzmann constant, and G is the ground heat flux (Wm^{-2}).

Neglecting transport of surface snow a cross grid cells due to avalanche and drift, the snow water content is computed as the balance between fresh snowfall, snowmelt, and sublimation:

$$\frac{\partial W_s}{\partial t} = P_{snow} - S_{melt} - E_s \quad (5)$$

where W_s is water-equivalent snow depth (m), P_{snow} is snowfall rate (ms^{-1}), E_s is the rate at which the snow layer gains or losses mass through sublimation (ms^{-1}), and S_{melt} is snowmelt rate (ms^{-1}). Snowmelt is computed as a part of the surface energy balance. If T_s obtained from the surface energy balance equation is above the freezing point over a snow-covered surface, then snow melts until T_s decreases to the freezing point or the snow completely disappears. T_s is adjusted by the amount of latent heat of fusion used to melt snow.

Evapotranspiration is computed as the sum of bare-soil evaporation, canopy evaporation, and transpiration. This calculation includes the effects of soil texture, soil moisture content, leaf-area index, solar radiation, air temperature, and humidity (Noilhan and Planton, 1989; Jacquemin and Noilhan, 1990). Details of the evapotranspiration calculation within the SPS model are presented by Kim and Ek (1995).

3. The East Asia hydrometeorology simulation

Fig. 3a illustrates the terrain of the East Asian domain. This domain is 5400 km × 4800 km with a 60 km × 60 km resolution on a Lambert–Conformal map projection. This region is characterized by high elevation areas of the Tibetan Plateau and the Altai Mountains in the western part of the domain. The central and eastern part of the domain includes flat terrain in eastern China and the Pacific Ocean. The area of interest in this study is the densely populated regions of eastern China, the Korean Peninsula, and the Japan Islands. This area is one of the world's major grain production regions, and has been historically vulnerable to frequent floods and droughts.

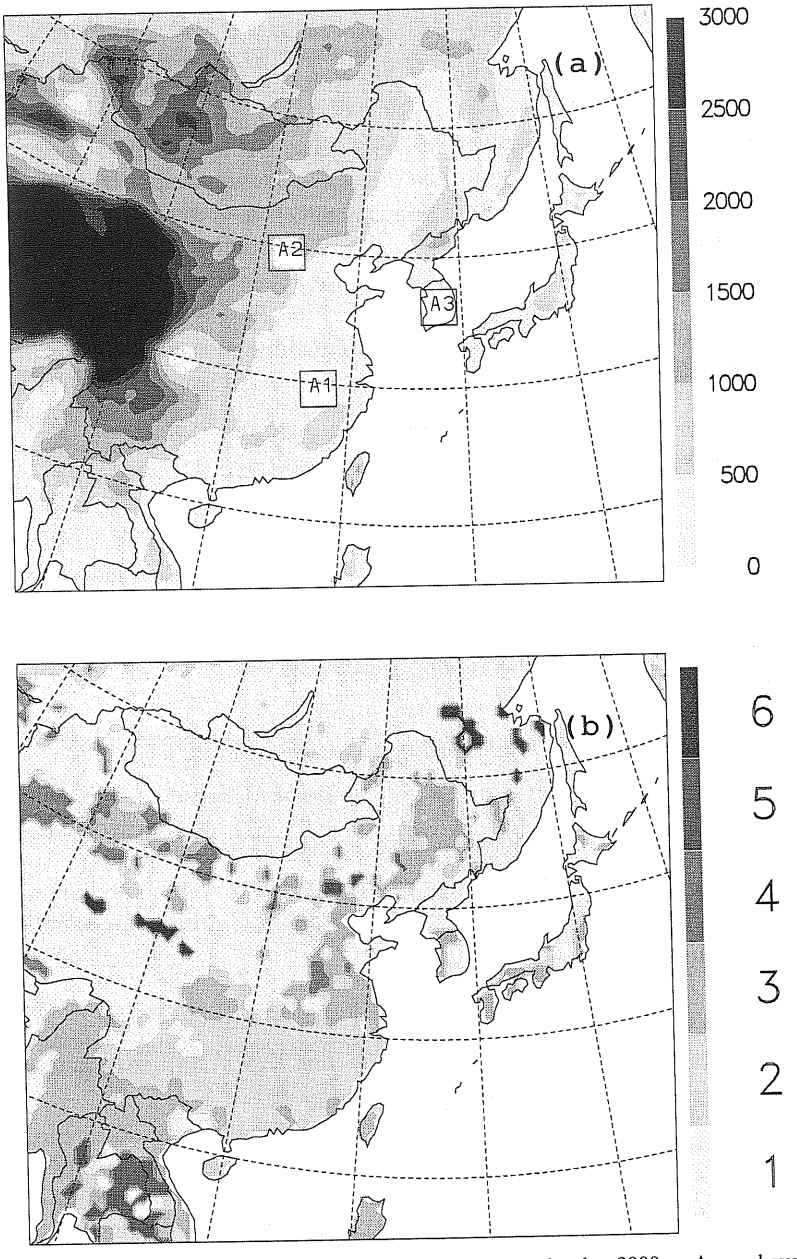

Fig. 3. (a) Terrain of the East Asian domain. Contour intervals are 500 m from the sea level to 3000 m. Areas above 3000 m above sea level are blacked. (b) Soil texture within the East Asian domain (1: Loam; 2: Silty-Clay; 3: Silty-Loam; 4: Loamy-Sand; 5: Sandy-Loam; 6: Silty-Clay–Loam).

One of the crucial requirements for regional hydroclimate simulations is a data base to provide land surface characteristics. The required information depends on the land surface scheme to be employed. The SPS model needs soil texture, green-leaf fraction (GLF), leaf-area index (LAI), and vertical distribution of root density. The coupled MAS-SPS model also can use spectral albedo, roughness length, and

zero-displacement height as a function of vegetation type if accurate data is available. In this study, we used the soil texture (Fig. 3b) of Zobler (1986). The GLF Fig. 4a and LAI (Fig. 4b) were obtained from Gutman and Iganov (1997) and the NASA/GSFC DAAC (1995), respectively. The GLF and LAI over the East Asian domain were prescribed by linearly interpolating the monthly-mean values. Due to a lack of data, we assumed that vegetation root density is uniform through the model soil layers.

Initial conditions and time-dependent lateral boundary conditions for this simulation were ob-

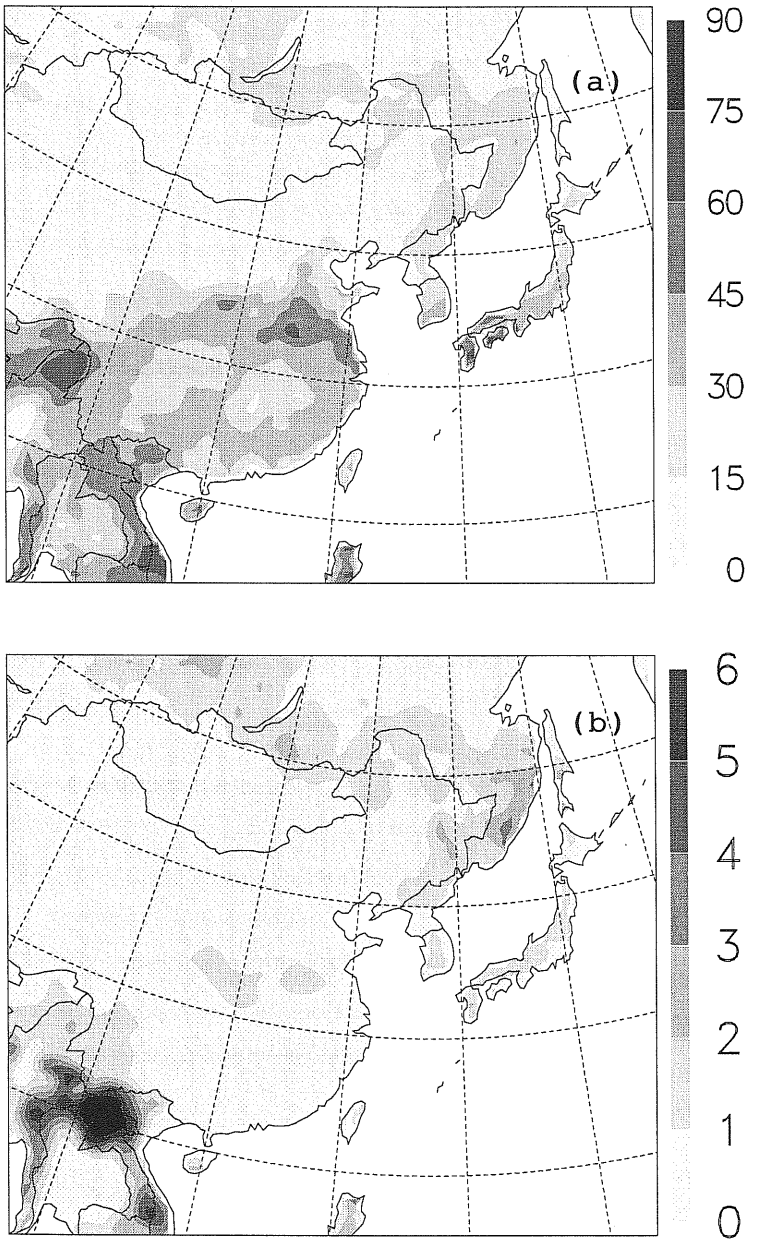

Fig. 4. April-mean values of (a) green-leaf fraction (%) and (b) leaf area index.

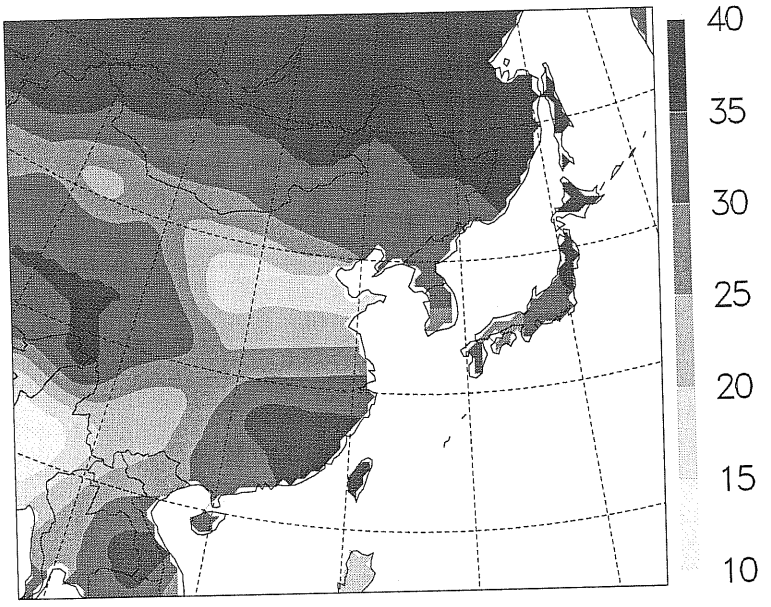

Fig. 5. Initial upper layer soil moisture content (vol.%) at 00UTC April 1, 1995 interpolated from the NCEP reanalysis data.

tained from the 2.5° × 2.5° resolution National Center for Environmental Prediction (NCEP) global reanalysis data (Kalnay et al., 1996). The global atmospheric fields were interpolated on the mesoscale model grid using the Cressman objective analysis scheme (Cressman, 1959). The reanalysis data set provides, in addition to the global atmospheric fields, global surface information at 6 h intervals. We used the reanalysis data to obtain initial fields for soil temperature, and soil moisture content (Fig. 5). The sea–surface temperature (SST) field was updated at 12 h intervals from the NCEP reanalysis SST data.

4. Results

The simulated and observed monthly-mean precipitation is presented in Fig. 6. The observed precipitation was obtained from the Global Precipitation Climatology Project (GPCP). During the spring season, precipitation in East Asia is usually associated with fast-moving polar lows from the north and the low pressure systems originating from southeastern slopes of the Tibetan Plateau, near Sichuan province. The simulated main precipitation band is located across the Yangtze River basin, East China Sea, and the Japan islands. The location and amount of the main precipitation band closely agrees with the GPCP data (Fig. 6b) and storm tracks (Fig. 7) during April 1995. Precipitation at the eastern Yangtze River Basin exceeded 10 mm/day. Snowfall occurred at the northern regions and high elevation areas during this period (not shown). Even though snowfall was light, it appears to have significantly affected surface albedo.

Soil moisture fields were closely correlated with simulated precipitation. Wet soil layers appear along the main precipitation band from the eastern part of the Yangtze River basin to the Japan Islands (Fig. 8). Soils were dry across central and western China and the Indo–China peninsula. Variation of the upper layer soil moisture during the simulation (Fig. 9) shows that major gain of soil moisture occurred along the main precipitation band, especially at the eastern Yangtze River basin. Significant drying of the upper soil layer occurred at the southern China, the Indo-China peninsula, and in the eastern Tibetan Plateau where precipitation was light. Deep soil moisture (not shown) changed more gradually, gaining moisture along the main precipitation band and losing elsewhere. Fig. 10 shows the response of the upper and lower layer soil moisture content to pre-

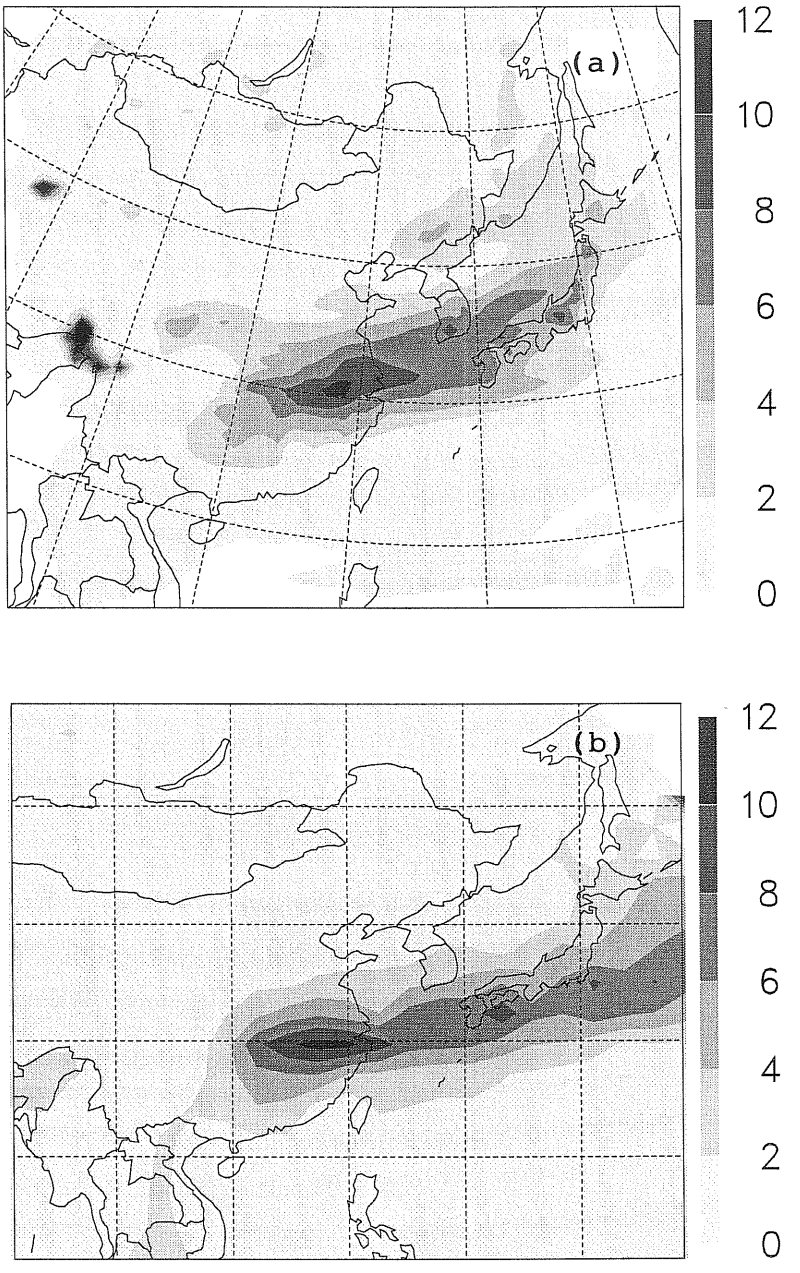

Fig. 6. Monthly-mean precipitation (mm/day) from (a) simulation and (b) GPCP data.

cipitation over a region at the eastern Yangtze River basin (A1 in Fig. 3a). During the first 12 days, soil moisture decreased in both layers. The upper soil layer moisture decreased about 1.5–times faster than the lower layer. As precipitation began on day-13, soil moisture at both soil layers increased in response to rainfall. The upper soil layer moisture rapidly fluctuated in response to rainfall events and quickly decreased after precipitation ended. The lower soil layer moisture continued to increase with each pre-

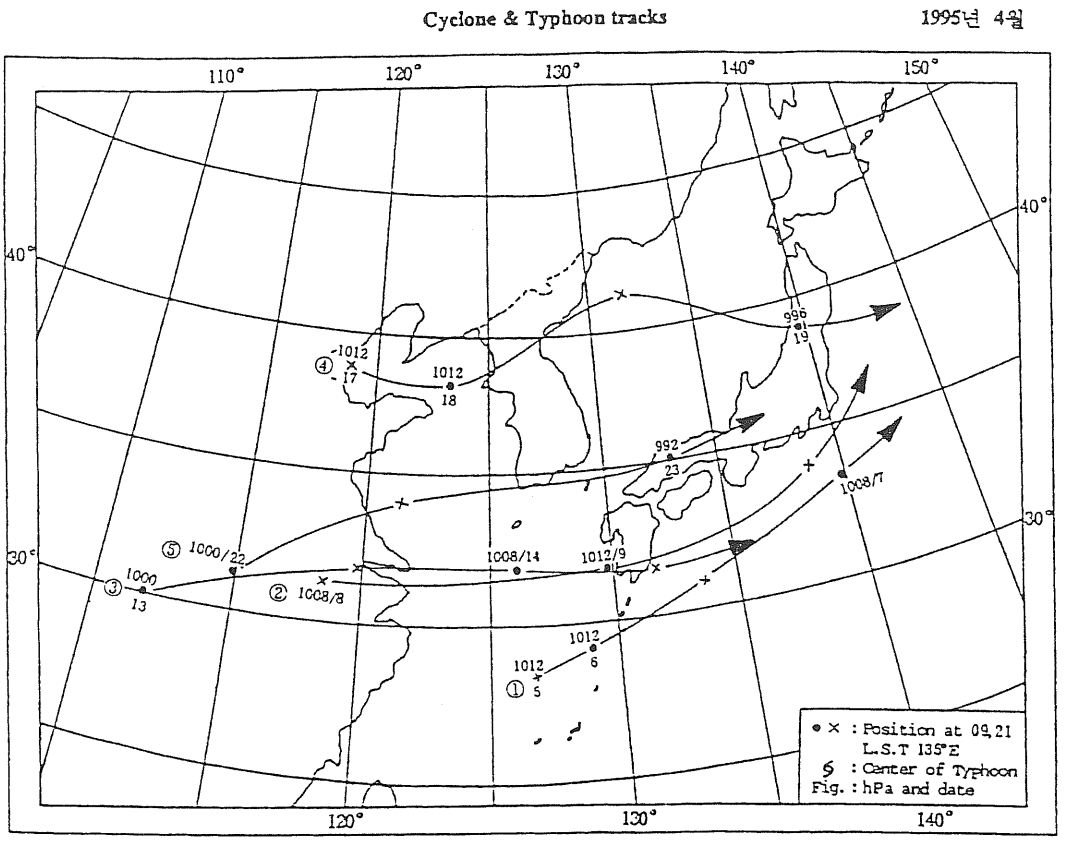

Fig. 7. Observed storm tracks in East Asia during April 1995 (Korean Meteorological Administration analysis).

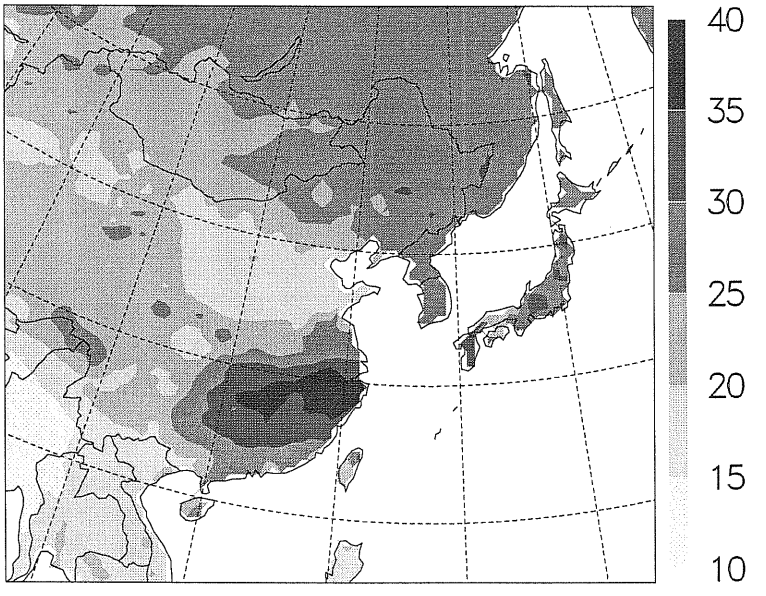

Fig. 8. Simulated monthly-mean soil moisture (vol.%) at the upper soil layer.

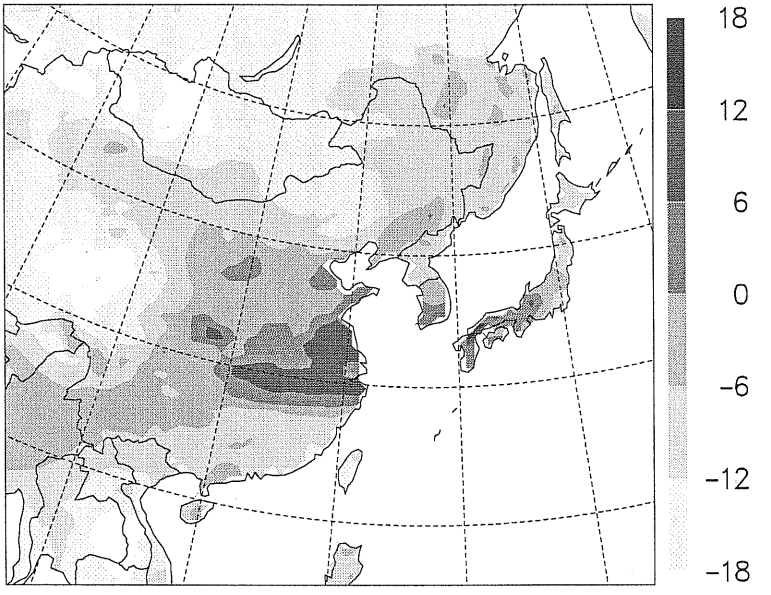

Fig. 9. Variation of upper layer soil moisture content (vol.%) during April 1995.

cipitation event. This implies that infiltration of soil moisture during precipitation events is much faster than the depletion of soil water due to transpiration which is the main cause of deep soil water loss over vegetated areas (Kim and Ek, 1995).

Radiation is the major forcing term in the land-surface energy budget. Detailed cloud microphysics and radiative transfer schemes, including formulations to account for effects of water and ice clouds on short- and longwave radiation, enable the MAS model to simulate physically-based radiative forcing fields. The simulated monthly-mean surface insolation (Fig. 11a) reflects the effects of cloud cover on surface insolation along the main precipitation band. Note that the monthly-mean surface insolation presented in Fig. 11a includes night time values. Weak surface insolation appeared along the main precipitation band where planetary albedo is also high (Fig. 11b). Weak surface insolation at high latitudes (north of 50° N) is due to a decrease of the solar zenith angle with increasing latitudes. Planetary albedo varied in response to cloud cover and surface snow cover. At low latitudes, positive anomaly of planetary albedo is due to cloud cover along the precipitation band. High albedo over the Tibetan Plateau, Mongolia, and Siberia is due to the presence of surface snow cover.

Local surface energy budgets were significantly affected by soil moisture content (Fig. 12). Over the wet soil surface of eastern Yangtze River basin (A1 in Fig. 3a), latent heat flux dominated sensible heat flux. Sensible heat flux dominates latent heat flux over the dry soil surface of northern China (A2 in Fig. 3a). Note that local noon for A1 and A2 is 04:30 UTC. One interesting feature of the surface energy budget is that soil heat flux was a significant compo-

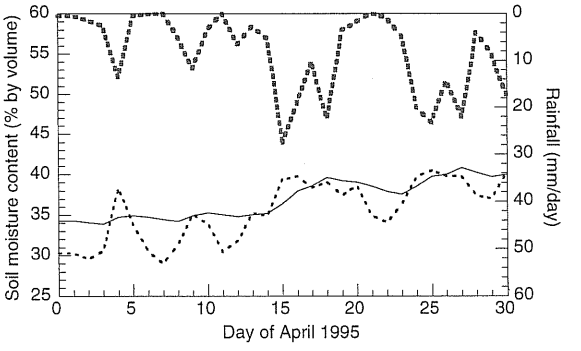

Fig. 10. Simulated daily precipitation and soil moisture over the area A1 in Fig. 3a. Note that precipitation is inverted.

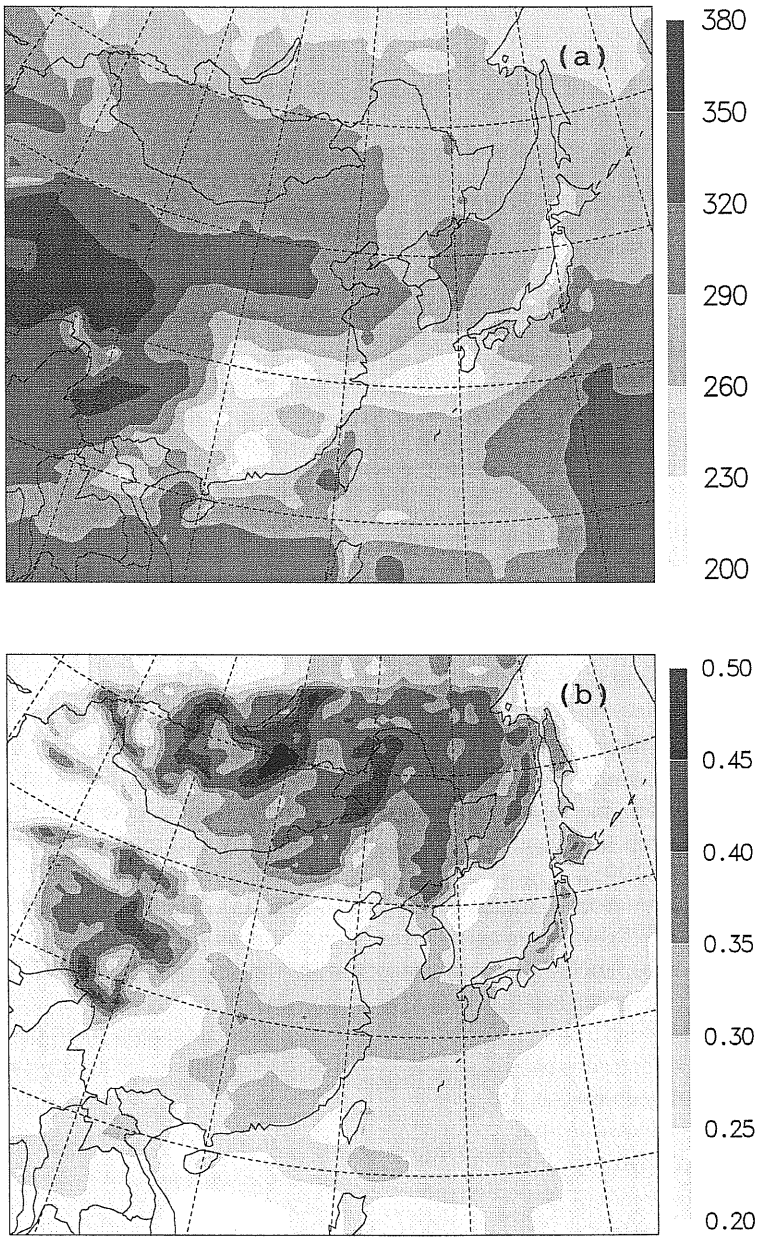

Fig. 11. Simulated (a) monthly-mean surface insolation (W/m^2) and (b) monthly-mean planetary albedo.

nent of the surface energy budget during this early spring season for both areas. Soil heat flux was about the same magnitude as the sensible heat flux and underwent a strong diurnal cycle (Fig. 12). This significance of soil heat flux may cause a difficulty in computing the surface energy budget, as it strongly depends on the temperature gradient and moisture content in the near-surface soil layer. In addition, few observations are available to evaluate the simulated soil heat flux term.

Despite its importance, obtaining an accurate soil moisture field over a large area is a difficult task.

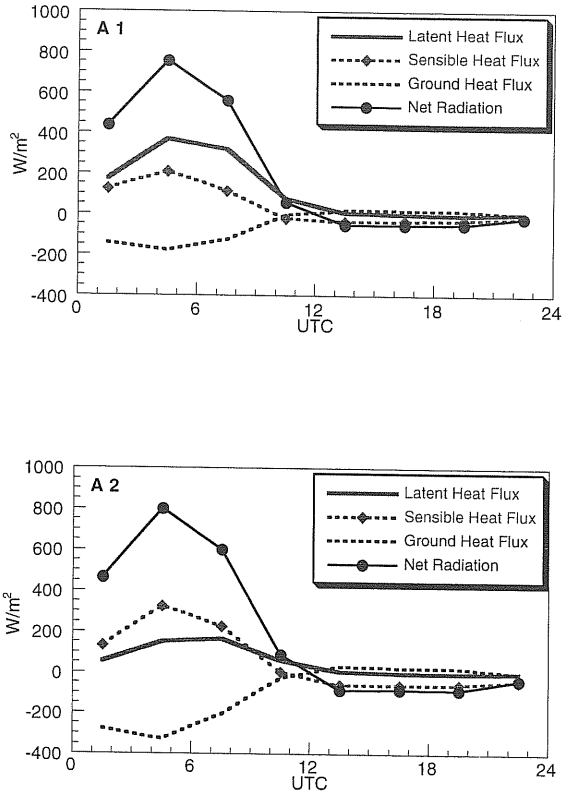

Fig. 12. Simulated diurnal cycle of the monthly-mean surface energy budget at areas A1 and A2 in Fig. 3a.

Therefore, a certain degree of uncertainty is unavoidable in prescribing soil moisture fields. Many off-line land surface modelling studies perform long-term spin–up simulations to obtain equilibrium states (e.g., Chen et al., 1997). Yang et al. (1995) found that the length of spin–up time in land surface models depends nonlinearly on parameters included in the model physics. Such an approach may not be used in coupled atmosphere–land surface modelling using historical data since feedback between the atmosphere and land surface may alter atmospheric forcing. A significant increase in the degree of freedom in a coupled model may cause delayed spin–up or spin–up into a different equilibrium state.

To investigate the effects of uncertainties in the initial soil moisture content on the simulated atmosphere–surface interactions, we carried out a sensitivity experiment in which the initial soil moisture field was set to 70% of the control simulation presented above. Even though reduction in the initial soil moisture field did not affect the general pattern of simulated fields (not shown), there was recognizable local effects in some areas. Location of the main rainband was shifted to the north by 1–2 grids over southern China. Over the Korean Peninsula and Japan Islands, the location of the main rainband did not change. Fig. 13 compares precipitation and upper

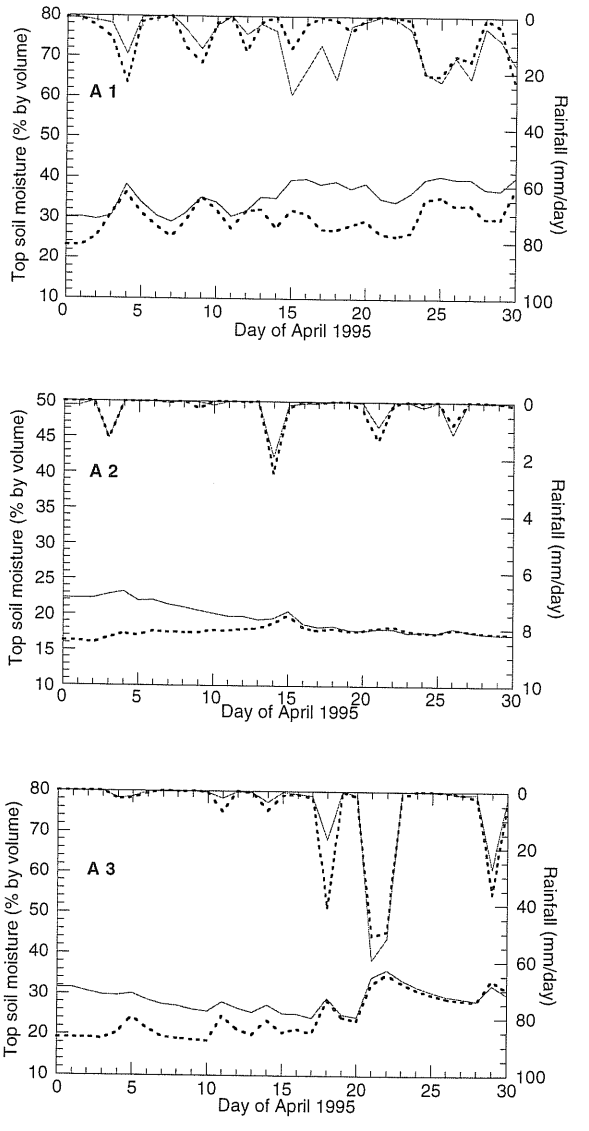

Fig. 13. Daily precipitation and upper layer soil moisture in the control simulation (solid line) and dry initial soil simulation (dashed line) at areas A1, A2, and A3 in Fig. 3a. Note that precipitation is inverted.

soil layer moisture variation from the two simulations at three locations (A1, A2, and A3 in Fig. 3a). The most significant effects of reduced initial soil moisture on precipitation appeared at southern China (A1), especially during the April 15–18 storm. At northern China (A2) and the Korean Peninsula (A3), effects of initial soil moisture on precipitation were relatively small. Upper layer soil moisture responded quickly to precipitation in both simulations. At northern China and Korean Peninsula, soil moisture in the two experiments converged to a common value during the second half of the simulation. Quick convergence of soil moisture from the two simulations is clear after each precipitation event. Soil moisture at southern China (A1) in the two simulations did not converge to a common equilibrium value even though they approach each other toward the end of the simulation. This may be caused by an alteration in the rainfall due to different initial soil moisture fields. At all three regions, the lower layer soil moisture from the two simulations was converging to each other, especially at the Korean Peninsula (not shown).

5. Conclusions

The Regional Climate System Model (RCSM) is an important tool for investigating regional climate variability and its impact on hydrology, water resources, and ecosystems. The coupled MAS–SPS model of the RCSM well simulated weather systems in eastern Asia during April 1995. The amount and location of the simulated precipitation agrees well with the observations. The main precipitation band was located across the Yangtze River basin, East China Sea, and the Japan Islands. Heaviest precipitation occurred at the eastern Yangtze River basin where rainfall maxima exceeded 10 mm/day. Orographic precipitation at the southern Korean Peninsula was well simulated.

Upper soil moisture rapidly varied in response to precipitation as it was marked by sharp increases during precipitation, followed by rapid decreases as precipitation ends. Lower layer soil moisture also sharply increased in response to precipitation. Decrease of soil moisture was much slower in the lower layer than in the upper layer. This suggests that infiltration into the deep soil layer during heavy precipitation is faster than the depletion of deep soil moisture by transpiration. During the study period, increases in soil moisture occurred along the main precipitation band. Major drying of soils occurred over the Indo–China peninsula and central–eastern China where precipitation was light.

The simulated solar radiation and planetary albedo were affected mostly by enhanced cloud cover along the main precipitation band and by the existence of surface snow cover at high latitudes. The simulated surface insolation near the precipitation maxima was, on the average, 30–60 Wm^{-2} below its surrounding relatively clear areas. As radiation is the main component of the surface energy budget, direct calculation of cloud optical properties and their impacts on radiative transfer using an explicit microphysics scheme is an important capability of the coupled MAS–SPS model for studying atmosphere–surface interactions.

The simulated surface energy budget suggests that soil moisture content is one of the most important factors controlling the surface energy budget. Latent heat flux dominated sensible heat flux over wet soil regions. Maximum overland evaporation occurred over the Yangtze River basin where the soil moisture content was highest despite reduced solar radiation due to cloud cover. Another important component in the surface energy budget was soil heat flux. The magnitude of soil heat flux was comparable to that of sensible heat flux during this early spring season.

The sensitivity experiment with reduced initial soil moisture content suggests that upper layer soil moisture field approaches an equilibrium value rather quickly after heavy precipitation events in most areas. However, in some areas, differences in the initial soil moisture field can be locally altered by the simulated rainfall. This in turn caused the soil moisture fields simulated with different initial values differ significantly from each other. This may introduce large uncertainties in short-term regional simulations.

Acknowledgements

The authors appreciate Mike Ek for providing Fig. 2 and for discussions toward the development of the SPS model. We also thank Prof. Sohn of Seoul

National University for regional precipitation data. Computational resources were provided by the San Diego Super Computing Center, the NASA Center for Computational Sciences, and the System Engineering Research Institute of Korea. This work was supported by the NASA MTPE grant W-19, 081, and by The Ministry of the Science and Technology of Korea under the grant PD-01-01-01. Work performed under the auspicies of U.S. DOE by the Lawrence Livermore National Laboratory under contract No. W-7405-Eng-48.

References

Anthes, R., 1977. A cumulus parameterization scheme utilizing a one-dimensional cloud model. Mon. Wea. Rev. 105, 270–286.

Arakawa, A., Suarez, M., 1983. Vertical differencing of the primitive equations in sigma coordinates. J. Atmos. Sci. 111, 34–45.

Avissar, R., Pielke, R., 1989. A parameterization of heterogeneous land surfaces for atmospheric numerical models and its impact on regional meteorology. Mon. Wea. Rev. 117, 2113–2136.

Bae, D.H., Georgakakos, K., 1994. Climatic variability of soil water in the American Midwest: 1. Hydrologic modelling. J. Hydrol. 162, 355–377.

Beven, K., Quinn, P., Romanowicz, R., Freer, J., Fischer, J., Lamb, R., 1994. TOPMODEL and GRIDATB: A users guide to the distribution versions. CRES Tech. Rep. TR110/94.

Chen et al., 1997.

Cho, H., Niewiadomski, M., Iribarne, J., 1989. A model of the effect of cumulus clouds on the redistribution and transformation of pollutants. J. Geophys. Res. 94 (D10), 12895–12910.

Cressman, G., 1959. An operational objective analysis system. Mon. Wea. Rev. 87, 367–374.

Cuenca, R., Ek, M., Mahrt, L., 1996. Impact of soil water property parameterization on atmospheric boundary layer simulation. J. Geophys. Res. 101 (D3), 7269–7277.

Davies, H., 1976. A lateral boundary formulation for multi-level prediction models. Q. J. Roy. Meteorol. Soc. 102, 404–418.

Deardorff, J., 1978. Efficient prediction of ground surface temperature and moisture, with inclusion of a layer of vegetation. J. Geophys. Res. 83 (C4), 1889–1903.

Dickinson, R., Henderson-Sellers, A., Kennedy, P., Wilson, M., 1986. Biosphere–atmosphere transfer scheme (BATS) for the NCAR community climate model. NCAR Tech. Note NCAR/TN-275+STR, 69 pp., NCAR, Boulder.

Dickinson, R., Errico, R., Giorgi, F., Bates, G., 1989. A regional climate model for the western United States. Climatic Change 15, 383–422.

Dickinson, R., Henderson-Sellers, A., Rosenzweig, C., Sellers, P., 1991. Evapotranspiration models with canopy resistance for use in climate models, a review. Agric. Forest Meteorol. 54, 373–388.

Fast, J., McCorcle, M., 1991. The effect of heterogeneous soil moisture on a summer baroclinic circulation in the central United States. Mon. Wea. Rev. 119, 2140–2167.

Giorgi, F., Bates, G., 1989. The climatological skill of a regional model over complex terrain. Mon. Wea. Rev. 117, 2325–2347.

Giorgi, F., 1991. Sensitivity of simulated summertime precipitation over the western United States to different physics parameterizations. Mon. Wea. Rev. 119, 2870–2888.

Giorgi, F., Bates, G., Nieman, S., 1993. The multiyear surface climatology of a regional atmospheric model over the western United States. J. Climate 6, 75–95.

Giorgi, F., Brodeur, C., Bates, G., 1994. Regional climate change scenarios over the United States produced with a nested regional climate model. J. Climate 7, 375–399.

Giorgi, F., 1995. Prospectives for regional earth system modelling. Global Planet. Change 10, 23–42.

Gutman, G., Iganov, A., 1997. Derivation of green vegetation fraction from NOAA/AVHRR for use in numerical weather prediction models. Int. J. Remote Sensing (to be published).

Harahvardahn, Davis, R., Randall, D., Corsetti, T., 1987. A fast radiation parameterization for atmospheric circulation models. J. Geophys. Res. 92 (D1), 1009–1016.

Henderson-Sellers, A., Pitman, A., 1992. Land-surface schemes for future climate models: specification, aggregation, and heterogeneity. J. Geophys. Res. 97 (D3), 2687–2696.

Jacquemin, B., Noilhan, J., 1990. Sensitivity study and validation of a land surface parameterization using the HAPEX-MOBILHY data set. Boundary Layer Meteorol. 52, 93–134.

Kalnay, E., Kanamitsu, M., Kistler, R., Collins, W., Deaven, D., Gandin, L., Iredell, M., Saha, S., White, G., Woollen, J., Zhu, Y., Chelliah, M., Ebisuzaki, W., Higgins, W., Janowiak, J., Mo, K., Ropelewski, C., Wang, J., Leetmaa, A., Reynolds, R., Jenne, R., Joseph, D., 1996. The NCEP/NCAR 40-year reanalysis project. Bull. Am. Meteorol. Soc. 77, 437–471.

Kim, J., Mahrt, L., 1992. Simple formulation of turbulent mixing in the stable free atmosphere and nocturnal boundary layer. Tellus A 44, 381–394.

Kim, J., Ek, M., 1995. A simulation of the surface energy budget and soil water content over the Hydrologic Atmospheric Pilot Experiments—Modélisation du Bilan Hydrique forest site. J. Geophys. Res. 100 (D10), 20845–20854.

Kim, J., Soong, S., 1996. A simulation of a Precipitation event in the western U.S. In: Ghan, S., Pennel, W., Peterson, K., Rykiel, E., Scott, M., Vail, L. (Eds.), Regional Impacts of Climate Change. Battelle Press.

Kim, J., Miller, N., Chung, J., Oh, J., 1997. A simulation of precipitation and land-surface water budget over the East Asia using the UC-LLNL Regional Climate System Model. Proc. 3rd Int. Study Conf. on GEWEX in Asia and GAME, Seogwipocity, Korea.

Lorenz, E., 1960. Energy and numerical weather prediction. Tellus 12, 364–373.

Louis, J., Tiedke, M., Gelevyn, J., 1981. A short history of the operational PBL-parameterization at ECMWF. Workshop on planetary boundary parameterization, ECMWF, 59–79.

Mahrt, L., Pan, H., 1984. A two-layer model of soil hydrology. Boundary Layer Meteorol. 29, 1–20.

Manabe, S., 1969. Climate and the ocean circulation: I. the atmospheric circulation and the hydrology of the Earth's surface. Mon. Wea. Rev. 97, 739–774.

Miller, N., 1995. A sensitivity of surface heat and moisture fluxes due to topographic slope and azimuth. J. Geophys. Res. 100 (D9), 18669–18685.

Miller, N., Kim, J., 1996. Numerical prediction of precipitation and river flow over the Russian River watershed during the January 1995 California storms. Bull. Am. Met. Soc. 77, 101–105.

Miller, N., Kim, J., Duan, J., 1997. The UC-LLNL regional climate system model: Southwestern United States and Eastern Asia Studies. In: Staniforth, A. (Ed.), Research activities in atmospheric and ocean modelling. WMO-TD-No. 792.

Mintz, Y., 1984. The sensitivity of numerically simulated climates to land-surface boundary conditions. In: Houghton, J. (Ed.), The Global Climate. Cambridge Univ. Press, 233 pp.

NASA/GSFC DAAC, 1995. Global data sets for land–atmosphere models. ISLSCP initiative 1: 1987–1988, Vol. 1–5, CD-ROM.

Noilhan, J., Planton, S., 1989. A simple parameterization of land surface processes for meteorological models. Mon. Wea. Rev. 117, 536–549.

Pan, H., Mahrt, L., 1987. Interaction between soil hydrology and boundary layer development. Boundary Layer Meteorol. 38, 185–202.

Pan, H., 1990. A simple parameterization scheme of evapotranspiration over land for the NMC Medium-Range Forecast Model. Mon. Wea. Rev. 118, 2500–2512.

Pielke, R., Cotton, W., Walco, R., Tremback, C., Nicholls, M., Moran, M., Wesely, D., Lee, F., Copland, J., 1992. A comprehensive meteorological modelling system-RAMS. Meteor. Atmos. Phys. 49, 69–91.

Pitman, A., 1988. A new parameterization of the land surface for use in general circulation models. PhD Thesis, 481 pp., Univ. of Liverpool, Liverpool, England.

Sellers, P., Mintz, Y., Sud, Y., Dalcher, A., 1986. A simple biosphere model (SiB) for use within general circulation models. J. Atmos. Sci. 43, 505–531.

Soong, S., Kim, J., 1996. Simulation of a heavy wintertime precipitation event in California. Climatic Change 32, 55–77.

Starr, D., Cox, S., 1985. Cirrus clouds: I. A cirrus cloud model. J. Atmos. Sci. 42, 2663–2681.

Stephens, G., 1978. Radiation profiles in extended water clouds: II. Parameterization schemes. J. Atmos. Sci. 35, 2123–2132.

Takacs, L., 1985. A two-step scheme for the advection equation with minimized dissipation and dispersion errors. Mon. Wea. Rev. 113, 1050–1065.

Timbal, B., Hahmann, A., Pitman, A., Qu, W., Henderson-Sellers, A., Slater, A., 1996. New developments in the project for intercomparison of land-surface parameterization schemes. EOS 78, 173–181.

Yang, Z., Dickinson, R., Henderson-Sellers, A., Pitman, A., 1995. Preliminary study of spin-up process in soil–vegetation–atmosphere transfer schemes with the first stage data of PILPS Phase 1a. J. Geophys. Res. 100 (D8), 16553–16578.

Zobler, L. 1986. A world soil file for global climate modelling. NASA Tech Memo. 87802.